J Mater Sci: Mater Electron (2022) 33:22469–22479

Comparative investigation between complex energy and transfer matrix techniques for quasi-energy states in heterostructure materials

Elkenany B. Elkenany[1,*] and A. M. Elabsy[1]

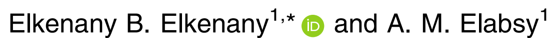

[1] *Department of Physics, Faculty of Science, Mansoura University, P.O. Box 35516, Mansoura, Egypt*

Received: 2 June 2022
Accepted: 29 August 2022
Published online:
13 September 2022

© The Author(s) 2022

ABSTRACT

A comparative analysis is performed to study the resonant tunneling through symmetric multiple double-barrier resonant tunneling heterostructure materials composed of nanoscale semiconductors ZnSe/BeTe, AlAs/GaAs, InGaAs/AlInAs, and AlGaAs/GaAs. Two techniques are applied in the present investigation for calculating the quasi-resonant energy states and their associated lifetimes in nanoscale double-barrier quantum well heterostructures. The first technique is based on the complex energy solution of the time-dependent Schrödinger equation with the time–energy uncertainty condition. The second one is employing the transfer matrix method. The quasi-resonant energies, lifetimes, and frequencies in nanoscale double-barrier quantum well heterostructures are calculated by both methods and compared. The validity and accuracy of both techniques are tested and compared extensively with various current numerical methods. Excellent agreements are obtained between our results and the available experimental and theoretical values. It is also found that the complex energy technique is recommended when handling the quasi-energy states and quasi-lifetimes of novel nanoscale devices.

1 Introduction

The recent modern techniques enabled bandgap engineering in semiconductor heterostructure materials to fabricate and enhance the performance of new optoelectronic devices based on III–V compounds and III nitride alloys [1]. These nanoscale devices such as quantum wells (double, triple, and multi-barriers), quantum dots, and quantum wires [2] have enormous applications in industry and daily life use [3]. Another novel fabricated nanostructures are the TiO_2 thin films that recommended for optical anti-counterfeiting applications [4, 5] and optoelectron devices [6]. The resonant tunneling phenomena in semiconductor devices attracted great attention. Over the past decades, resonant tunneling heterostructures (RTHSs) have been widely used for studying fundamental physical processes and developing novel and high-speed functional devices. Most of the early studies were focused on double-barrier RTHSs

Address correspondence to E-mail: kena@mans.edu.eg

https://doi.org/10.1007/s10854-022-09025-8

(DBRTHSs), which consist of a quantum well confined by two thin barriers and a pair of contacts. The resonant quasi-level lifetime or frequency is one of the most important issues concerning the development of novel nanoscale electronic devices. Resonant transmission probability in different semiconductor heterostructures having extremely narrow dimensions in presence of electric bias has been investigated following the pioneering works by Esaki and Tsu [7]. Various numerical techniques are adopted thereafter by eminent researchers for near accurate computational purposes, like variational method [8], Airy's function approach [9], weighted potential method [10], finite element method [11], and transfer matrix technique (TMT) [12–14]. Transmission coefficients were computed for triple-barrier heterostructures [15–19] in the presence and absence of an electric field. This technique was extended for the analysis of superlattice nanostructures [20, 21]. Elabsy and Elkenany [22] studied the effect of the nonparabolicity on the resonant lifetimes and resonant energies of symmetric GaAs/$Al_xGa_{1-x}As$ double-barrier nanostructures.

The present work performs a comparative theoretical analysis for calculating the quasi-resonant energies and their associated quasi-resonant lifetimes in nanoscale double-barrier heterostructures in the absence of an electric field. The complex energy method and the transfer matrix technique are employed and compared in the present computations. We consider atomic units in which $m_0 = e = \hbar = 1$.

2 Mathematical modeling

2.1 Transfer matrix technique

Figure 1 shows the heterostructure materials composing the DBRTHS for this technique in which the horizontal z-axis is chosen as the growth direction and the vertical axis stands for the potential barrier V(z) that arises from the bandgap discontinuity at the interface of the two heterostructure materials with height V_0.

The calculations are based on the transfer matrix method. The analysis takes into its account the total energy and the transverse motion of the charged carriers (electrons/holes) that is represented by the thermal energy (which equals k_BT, where T is the absolute temperature given in Kelvin and k_B is the Boltzmann constant). The transmission coefficient, $T_r(E)$, for DBRTHS is determined from the relation [23, 24]:

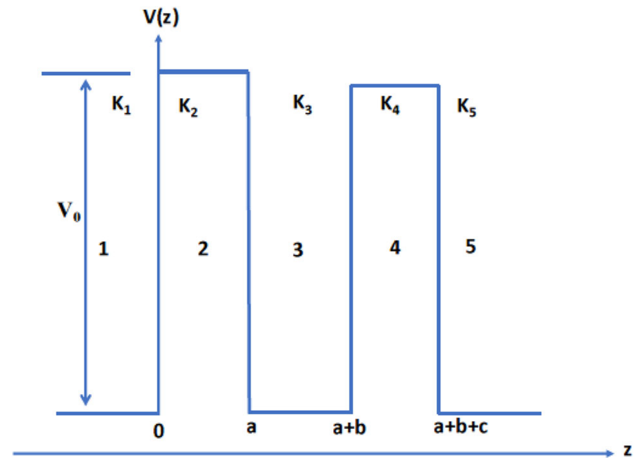

Fig. 1 Schematic representation of double-barrier heterostructure semiconductors, a and c are the barrier thicknesses, and b is the width of the quantum well

$$T_r(E) = \frac{4}{\left[(\zeta_{11}+\zeta_{22})^2 + \left(k_1\zeta_{12} - \frac{\zeta_{21}}{k_1}\right)^2\right]}, \quad (1)$$

where

$$\zeta_{11} = \cosh(k_2a)\left[\cosh(k_2c)\cos(k_1b) - \frac{k_1\gamma}{k_2}\sinh(k_2c)\sin(k_1b)\right] + \frac{k_2}{\gamma}\sinh(k_2a)\left[\frac{1}{k_1}\cosh(k_2c)\sin(k_1b) + \frac{\gamma}{k_2}\sinh(k_2c)\sin(k_1b)\right] \quad (2)$$

$$\zeta_{12} = \frac{\gamma}{k_2}\sinh(k_2a)\left[\cosh(k_2c)\cos(k_1b) - \frac{k_1\gamma}{k_2}\sinh(k_2c)\sin(k_1b)\right] + \cosh(k_2a)\left[\frac{1}{k_1}\cosh(k_2c)\sin(k_1b) + \frac{\gamma}{k_2}\sinh(k_2c)\cos(k_1b)\right] \quad (3)$$

$$\zeta_{21} = \cosh(k_2a)\left[\frac{k_2}{\gamma}\sinh(k_2a)\cos(k_1b) - k_1\cosh(k_2a)\sin(k_1b)\right] + \frac{k_2}{\gamma}\sinh(k_2a)\left[\frac{k_2}{\gamma k_1}\sinh(k_2a)\sin(k_1b) + \cosh(k_2a)\cos(k_1b)\right] \quad (4)$$

$$\zeta_{22} = \frac{\gamma}{k_2}\sinh(k_2a)\left[\frac{k_2}{\gamma}\sinh(k_2c)\cos(k_1b) - k_1\cosh(k_2c)\sin(k_1b)\right] + \cosh(k_2a)\left[\frac{k_2}{\gamma k_1}\sinh(k_2c)\sin(k_1b) + \cosh(k_2c)\cos(k_1b)\right]. \quad (5)$$

One obtains a general form of the full width at half maximum, FWHM of the resonant energy peak to determine the lifetime at the resonance energy, E_{rn} (n is the peak order) by applying the time–energy uncertainty condition as

$$\tau_n = \frac{\hbar}{2\Delta E_n}, \tag{6}$$

where $2\Delta E_n$ is the FWHM of the resonant transmission peak which is given by [23]

$$|2\Delta E_n| = \frac{32E_{rn}\sqrt{(V_0 - E_{rn})/E_{rn}}}{\left[2 + \alpha_3\sqrt{\frac{V_0 - E_{rn}}{E_{rn}}}\right]} \cdot \frac{(V_0 - E_{rn})E_{rn}e^{-2\alpha_2}}{V_0^2} \tag{7}$$

$$\alpha_2 = k_2 c, \alpha_3 = k_3 b \tag{8}$$

$$k_1 = k_3 = k_5 = \sqrt{2m_1^*[E - E_t]} \tag{9}$$

$$k_2 = k_4 = \sqrt{2m_2^*\left\{V_0 - \left(E - \frac{E_t}{\gamma}\right)\right\}} \tag{10}$$

$$\gamma = \frac{|m_2^*|}{|m_1^*|}. \tag{11}$$

In the above equations E is the total energy, while E_t is the transverse energy.

2.2 Complex energy technique

Figure 2 depicts the heterostructure materials composing the DBRTHS for the complex energy technique in which the origin of the growth direction, the z-axis, is at the center of the quantum well and V_0 is the height of the potential barrier V(z).

2.2.1 For even-quasi-states

One obtains the transcendental energy equation that gives the allowed 1st, 3rd, …, etc. quasi-resonant energies as [19, 21, 22]

$$\frac{\chi\cot(\zeta)}{\gamma\zeta} + \frac{\chi[1 + e^{2\delta\chi}] + i\gamma\zeta[1 - e^{2\delta\chi}]}{\chi[1 - e^{2\delta\chi}] + i\gamma\zeta[1 + e^{2\delta\chi}]} = 0, \tag{12}$$

where

$$\zeta = k_1 a \tag{13}$$

$$\delta = \frac{b}{a} = \frac{\text{barrier thickness}}{\text{half well thickness}} \tag{14}$$

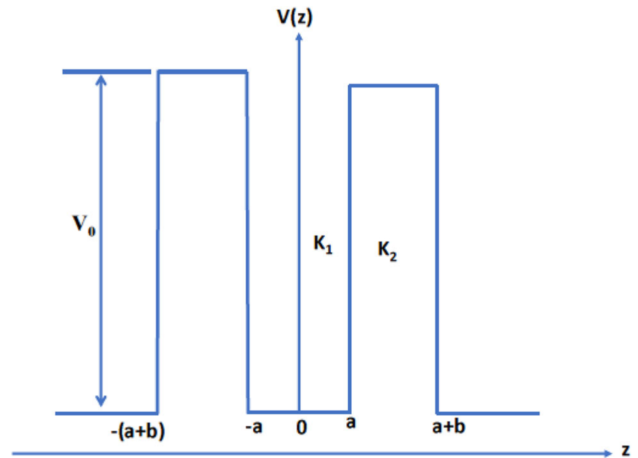

Fig. 2 Schematic representation of the double-barrier heterostructure semiconductors. b is the barrier thickness and a is the half-width of the quantum well

$$\mathcal{X} = k_2 a = \begin{cases} \sqrt{(U_i - \gamma\zeta^2)}, & \text{for} \quad \text{Re}(\zeta^2) < \frac{U_i}{\gamma} \\ i\sqrt{(\gamma\zeta^2 - U_i)}, & \text{for} \quad \text{Re}(\zeta^2) > \frac{U_i}{\gamma} \end{cases} \tag{15}$$

$$U_i = 2m_2^* a^2 V_0. \tag{16}$$

2.2.2 For odd-quasi-states

The transcendental energy equation that gives the allowed 2nd, 4th, …, etc. quasi-resonant energies has the form [19, 21, 22]

$$\frac{\chi\tan(\zeta)}{\gamma\zeta} - \frac{\chi[1 + e^{2\delta\chi}] + i\gamma\zeta[1 - e^{2\delta\chi}]}{\chi[1 - e^{2\delta\chi}] + i\gamma\zeta[1 + e^{2\delta\chi}]} = 0. \tag{17}$$

The solutions (roots) of Eqs. (12) and (17), η_n are complex which computed numerically with n is the root order that equals n = 1, 3, …, etc. for even quasi-energy states (Eq. 12) and n = 2, 4, …, etc. for the odd quasi-energy states (Eq. 17). The imaginary part of these roots is related to the resonant energy width, which is associated with the quasi-resonant lifetime, τ_n. Follow the same manipulations as in Refs. [22, 25–27], we obtain the n quasi-lifetime τ_n as

$$\tau_n = \frac{-1}{2\omega_n Im(\eta_n^2)}. \tag{18}$$

The imaginary part of energy satisfies the time–energy uncertainty principle, $\tau_n = \hbar/\in$ with $\hbar = 1$ and $\in = -2\omega_n Im(\eta_n^2)$.

3 Results and discussion

The present calculations are applied to nanoscale DBRTHS materials composed of different semiconductors as follows.

3.1 ZnSe/BeTe

The heterostructure semiconductors composed of the system ZnSe/BeTe are presented as shown in Fig. 1 with ZnSe as the well region and BeTe as the barrier region. Figure 3 displays that the variation of the natural logarithm of the transmission coefficients as a function of the resonant electron energy for nanoscale ZnSe/BeTe DBRTHS at T = 4.2 K with $m_1 = m_2 = 0.17$ and a height of the barrier $V_0 = 2.3$ eV for BeTe barrier thickness "b" of 6 nm and ZnSe well width "a" of 6 nm. Seven resonant peaks appear in the transmissivity which represents the resonant peaks and occurred at the quasi-energy states as listed in Table 1. The results of the quasi-resonant energies for both methods are computed by employing Eqs. (1), (12), and (17). The lifetimes τ_n values for charged carriers (electrons) are calculated by applying the peak fit program and the uncertainty relation given by Eq. (6). Table 1 lists the quasi-resonant energy, quasi-resonant lifetime, and quasi-resonant frequency that are calculated by the two different methods, complex energy method and transfer matrix method for the nanoscale ZnSe/BeTe DBRTHS at T = 4.2 K for $m_1 = m_2 = 0.17$ and a barrier height $V_0 = 2.3$ eV. There is an excellent agreement between the present work results and the experimental data given by Lunz et al. [28].

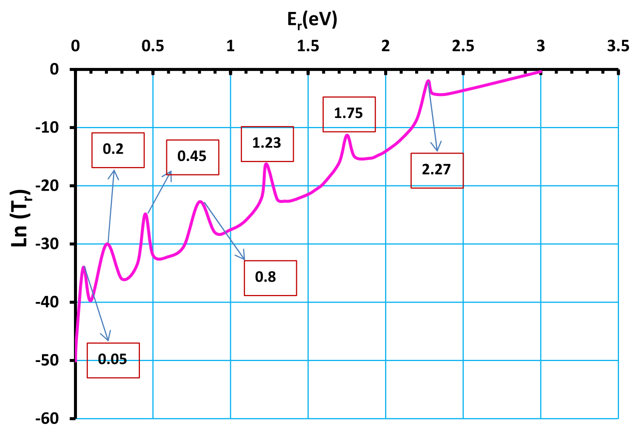

Fig. 3 Natural logarithmic transmission coefficients for nanoscale ZnSe/BeTe double-barrier heterostructures versus quasi-resonant energy at T = 4.2 K for $m_1 = m_2 = 0.17$ and a height of the barrier $V_0 = 2.3$ eV for a barrier thickness of 6 nm and a well width of 6 nm

Figure 4 displays the variation of the base 10 logarithmic quasi-resonant lifetimes for the nanoscale ZnSe/BeTe DBRTHS with the quasi-resonant energy at T = 4.2 K for $m_1 = m_2 = 0.17$, a barrier height $V_0 = 2.3$ eV, a barrier thickness of 6 nm, and a well width of 6 nm for the complex energy and transfer matrix methods. The solid line is related to the transfer matrix method, while the dashed line involves the complex energy method. In Fig. 4, the quasi-resonant lifetime decreases by increasing the quasi-resonant energy, and the lifetimes associated with both the complex energy method and transfer matrix technique are given in Table 1. It is evident from Fig. 4 and Table 1 that the calculated results for both methods are in good accordance with each other.

Table 1 Quasi-resonant energy, E_{rn} (eV), quasi-resonant lifetime, τ_n (s), and quasi-resonant frequency, f_n (Hz), for nanoscale ZnSe/BeTe double-barrier heterostructures at T = 4.2 K as functions of resonant energy for $m_1 = m_2 = 0.17$ and a barrier height $V_0 = 2.3$ eV for a barrier thickness of 5 nm and a well width of 6 nm

Present work						Experiment Ref [28]
Complex energy technique			Transfer matrix method			
E_r (eV)	τ_n(s)	f_n (Hz)	E_r (eV)	τ_n (s)	f_n (Hz)	E_r (eV)
0.05037	3.4456	0.290225	0.05	1.08E3	9.26E − 04	0.05
0.20105	0.1578	6.337136	0.2	4.01E1	2.49E − 02	0.2
0.45061	8.23E − 03	121.5067	0.45	1.43	6.99E − 01	0.45
0.79611	2.59E − 04	3861.004	0.8	2.45E − 2	4.08E + 01	0.8
1.2317	3.30E − 06	303,030.3	1.23	1.50E − 4	6.67E + 03	1.23
1.74377	9.07E − 09	1.1E + 08	1.75	1.13E − 7	8.85E + 06	1.75
2.2693	9.01E − 13	1.11E + 12	2.27	1.53E − 12	6.54E + 11	2.27

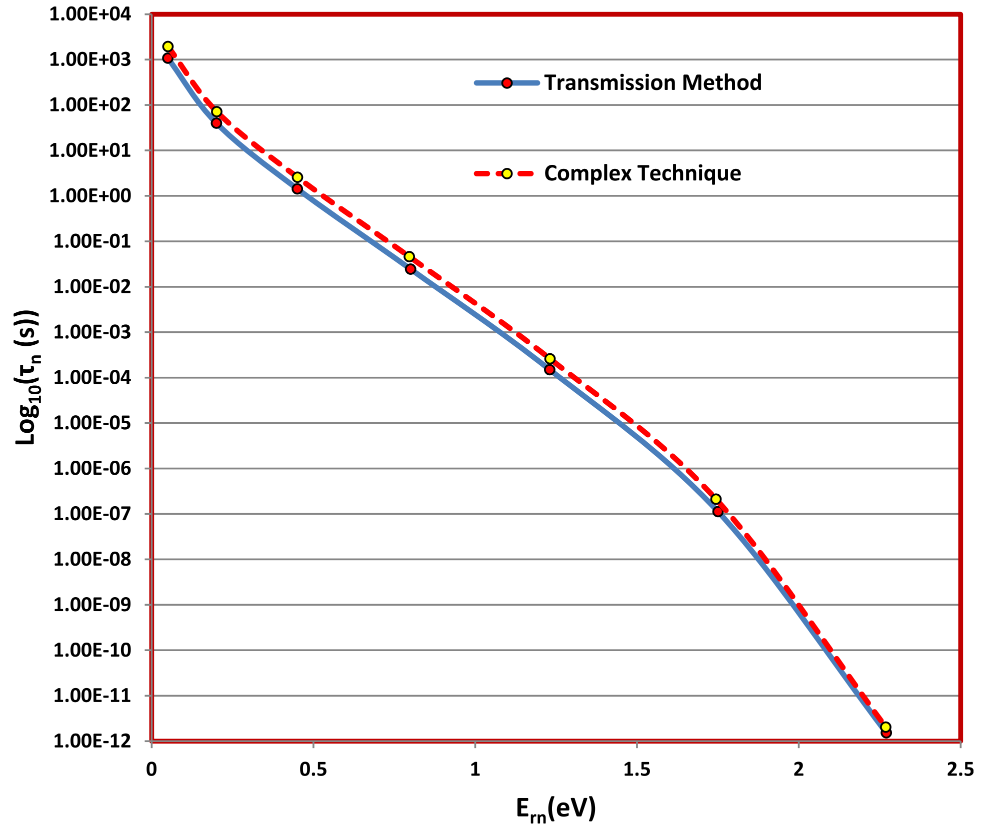

Fig. 4 Logarithmical base 10 of quasi-resonant lifetimes for nanoscale ZnSe/BeTe double-barrier heterostructures at T = 4.2 K as a function of quasi-resonant energy for $m_1 = m_2 = 0.17$, the height of the barrier $V_0 = 2.3$ eV for a barrier thickness of 6 nm, and a well width of 6 nm by two different methods, solid line (Transfer matrix method) and dashed line (Complex energy method)

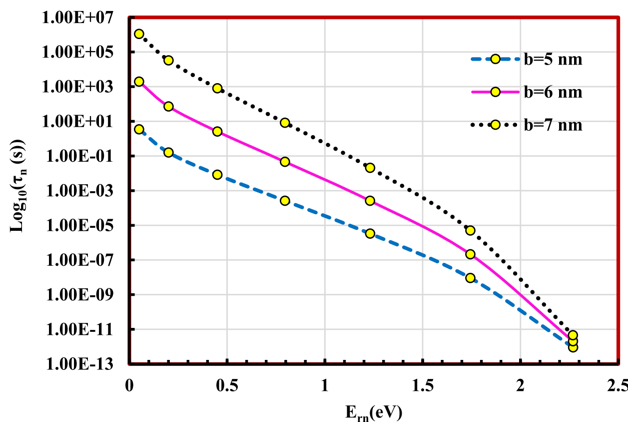

Fig. 5 Logarithmical base 10 quasi-resonant lifetimes for ZnSe/BeTe double-barrier heterostructures at T = 4.2 K as a function of quasi-resonant energy for $m_1 = m_2 = 0.17$ and a height of the barrier $V_0 = 2.3$ eV for a well width of 6 nm for different values of barrier thickness 5, 6, and 7 nm

Figure 5 shows the natural logarithm of the quasi-resonant lifetime for nanoscale ZnSe/BeTe double-barrier heterostructures as a function of the quasi-resonant energy at T = 4.2 K for $m_1 = m_2 = 0.17$, a barrier height of $V_0 = 2.3$ eV, a well width of 6 nm, and for different values of the barrier thickness 5, 6, and 7 nm. In Fig. 5 the quasi-resonant lifetime at a constant (specific) quasi-resonant energy state enhances by increasing the barrier thickness. This result is because increasing the barrier thickness diminishes the probability of penetrating the barrier by electrons and so increases the lagging time in penetrating the barrier to cross it to the neighboring well. Also, at a constant barrier thickness the quasi-lifetime decreases by increasing the quasi-resonant energy, this is because the enhancement of resonant energy leads to higher resonant energy states which in turn diminish the lifetime according to the uncertainty time–energy relation. Furthermore, raising the energy makes the resonant peaks flat and their energy spacing becomes broader and the full energy width at half maximum ($2\Delta E_n$) increases, so the resonance lifetime decreases according to the formula $1/2\Delta E_n$ as given in Eq. 6.

Figure 6 depicts the variation of the base 10 logarithms of quasi-resonant frequencies for the nanoscale ZnSe/BeTe double-barrier heterostructures with quasi-resonant energy at T = 4.2 K for $m_1 = m_2 = 0.17$, a barrier height of $V_0 = 2.3$ eV, and a well width of 6 nm for different values of barrier thickness

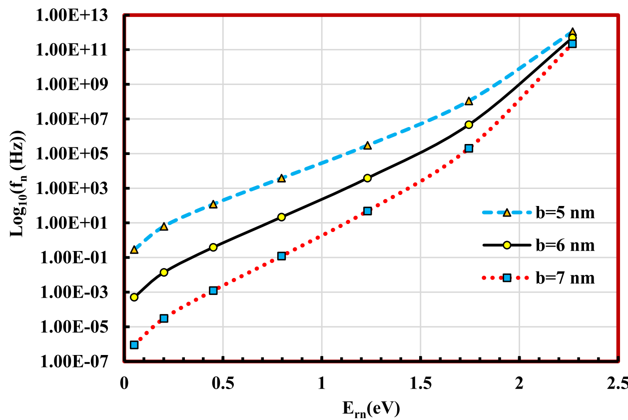

Fig. 6 Logarithmical base 10 of the quasi-resonant frequencies for ZnSe/BeTe double-barrier heterostructures as a function of quasi-resonant energy at T = 4.2 K for $m_1 = m_2 = 0.17$, a height of the barrier $V_0 = 2.3$ eV, and a well width of 6 nm for different values of barrier thickness 5, 6, and 7 nm

5, 6, and 7 nm. From Fig. 6, the quasi-resonant frequency enhances by increasing the quasi-resonant energy and decreases by increasing the barrier thickness. This finding is because enhancing the barrier thickness increases the quasi-lifetime which in turn increases the quasi-frequency for electrons (due to the inverse time–frequency relation). The resonant peaks become flatter and their energy spacings become wider with increasing energy. Thus, the energy width at half maximum ($2\Delta E_n$) enhances so the resonance frequency increases as $\tau_n = 1/f_n$ decreases.

3.2 GaAs/AlAs

The heterostructure semiconductors composed of the system GaAs/AlAs are presented as shown in Fig. 1 with GaAs as the well region and AlAs as the barrier region. We computed the quasi-resonant energies and their associated quasi-lifetimes for the complex energy and the transfer matrix techniques for different nanoscale GaAs/AlAs heterostructures. Table 2 displays the results computed for the nanoscale GaAs/AlAs double-barrier heterostructures with parameters a = 6.2 nm and $m_1 = m_2 = 0.069$ for two barrier heights $V_0 = 0.96$ and 1.36 eV with different values of barrier thickness. Excellent agreement is obtained between the present work and the corresponding published data by Xu and Okada [29]. Furthermore, the results for both the complex energy and transfer matrix methods are in excellent accordance. Figure 7 shows the natural logarithm of transmission coefficients for nanoscale AlAs/GaAs double-barrier heterostructures versus quasi-resonant energy at nearly room temperature, T = 300 K for $m_1 = m_2 = 0.069$ for two barrier heights $V_0 = 0.96$ and 1.36 eV with barrier thickness of 2.8, 3.4, and 4.0 nm and a well width of 6.2 nm. In Fig. 7, there is a single resonant peak that appears in the

Table 2 Calculated quasi-resonant energies and quasi-lifetimes for nanoscale AlAs/GaAs double-barrier heterostructures for a = 6.2 nm, $m_1 = m_2 = 0.069$, and $V_0 = 0.96$ eV and 1.36 eV for different values of barrier thickness

b(nm)	Present work				Ref. [29] τ_n (ps)
	Complex energy method		Transfer matrix technique		
	E_r (eV)	τ_n (ps)	E_r (eV)	τ_n (ps)	
$V_0 = 0.96$ eV					
2.8	0.090877	9.39	0.117	9.39	9.38
3.4	0.0909153	42.32	0.117	42.32	42.30
4.0	0.09092369	190.71	0.117	190.72	190.63
$V_0 = 1.36$ eV					
2.8	0.0971304	48.01	0.123	48.05	47.90
3.4	0.097140	294.77	0.123	294.89	294.65
4.0	0.0971415	1809.80	0.123	1809.78	1809.07

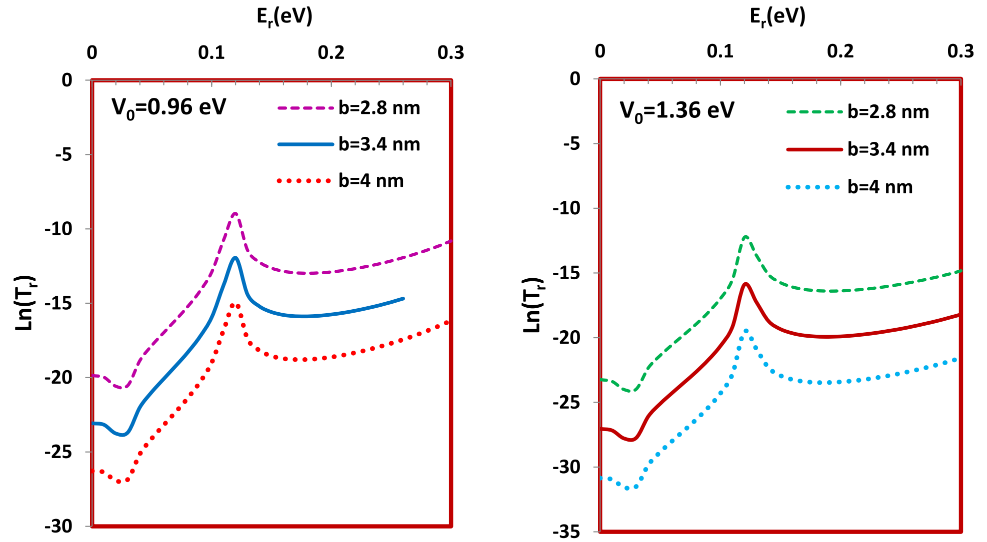

Fig. 7 Natural Logarithmic transmission coefficients for AlAs/GaAs double-barrier heterostructures versus quasi-resonant energy at T = 300 K for $m_1 = m_2 = 0.069$, for (a) $V_0 = 0.96$ eV and (b) $V_0 = 1.36$ eV with barrier thickness of 2.8, 3.4, and 4.0 nm and a well width of 6.2 nm

transmissivity for each value of the barrier thickness. Table 2 presents the values obtained from Fig. 7 for the resonant peaks and their associated lifetimes. The calculated values for both techniques are in excellent accordance with each other and with the published data [29].

3.3 InGaAs/AlInAs

The heterostructure semiconductors composed of the system InGaAs/AlInAs are presented as shown in Fig. 1 with InGaAs as the well region and AlInAs as the barrier region. The calculated resonant energies and lifetimes for nanoscale InGaAs/AlInAs double-barrier heterostructures with a = 6.0 nm, $m_1 = m_2 = 0.041$, and $V_0 = 0.5$ eV for different values of barrier thickness are presented in Table 3. The calculated results from both methods are in excellent agreement with each other and with the published data in Ref. [29]. Figure 8 exhibits the dependence of the natural logarithm of the transmission coefficients for InGaAs/AlInAs double-barrier heterostructures upon the quasi-resonant energy at T = 300 K with $m_1 = m_2 = 0.041$ and $V_0 = 0.5$ eV for barrier thickness of 4.0 and 7.0 nm and a well width of 6.0 nm. In Fig. 8 there is a single resonant peak that appears in the transmissivity for each value of the barrier

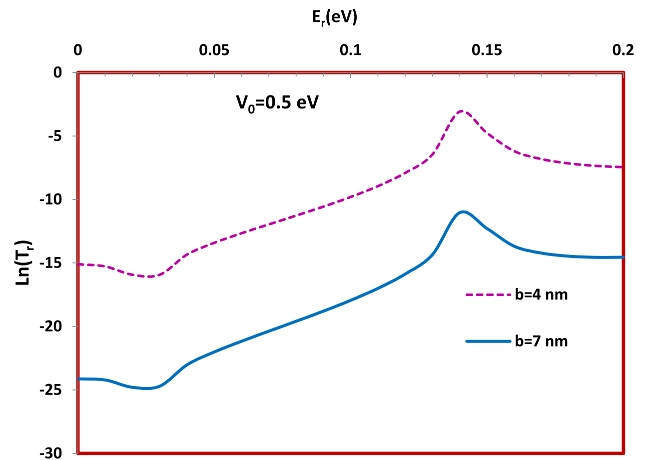

Fig. 8 Natural Logarithmic transmission coefficients for nanoscale InGaAs/AlInAs double-barrier heterostructures versus quasi-resonant energy at T = 300 K for $m_1 = m_2 = 0.041$ and $V_0 = 0.5$ eV for barrier thickness 4.0 nm and 7.0 nm and a well width of 6.0 nm

Table 3 Calculated quasi-resonant energies and quasi-lifetimes for nanoscale InGaAs/AlInAs double-barrier heterostructures for a = 6.0 nm, $m_1 = m_2 = 0.041$, and $V_0 = 0.5$ eV for different values of barrier thickness

b(nm)	Present work				Ref. [29] τ_n (ps)
	Complex energy method		Transfer matrix technique		
	E_r (eV)	τ_n (ps)	E_r (eV)	τ_n (ps)	
4.0	0.1168	0.539	0.140	0.541	0.539
7.0	0.1172	25.30	0.145	25.28	25.29

thickness. The quasi-resonant peaks occur at nearly $E_1 = 0.14$ eV and the associated lifetimes are $\tau_1 = 0.541$ ps, and 25.28 ps for b = 4.0 and 7.0 nm, respectively.

3.4 AlGaAs/GaAs

The heterostructure semiconductors composed of the system AlGaAs/GaAs are presented as shown in Fig. 1 with GaAs as the well region and AlGaAs as the barrier region. Table 4 lists the calculated quasi-resonant energy and their associated quasi-lifetimes obtained for nanoscale AlGaAs/GaAs double-barrier structure for a = 5.0 nm, b = 2.0 nm, $m_1 = 0.067$, $m_{2-} = m_1 + 0.083 \times$ with x = 0.5, and a potential height $V_0 = 0.5$ eV. Our results are in good agreement with those obtained by the recently used numerical methods [29]. Figure 9 displays the dependence of the natural logarithm of transmission coefficients for $Al_xGa_{1-x}As$/GaAs double-barrier structure upon resonant energy at T = 300 K for a = 5.0 nm, b = 2.0 nm, $m_1 = 0.067$, $m_2 = m_1 + 0.083 \times$ with Al mole fraction, x = 0.5, and $V_0 = 0.5$ eV. In Fig. 9 there are two resonant peaks appearing in the transmissivity for the value of the barrier thickness of 2.0 nm. The values of the resonant peaks and their associated lifetimes are given in Table 4. These values fairly agree well with that related to the complex energy technique and with the experimental values [29].

The obtained resonant energies and lifetimes for nanoscale AlGaAs/GaAs double-barrier heterostructures for another composition a = 5.0 nm, b = 5.0 nm, $m_1 = m_2 = 0.067$, and $V_0 = 0.23$ eV are listed in Table 5 and displayed in Fig. 10. Figure 10 depicts a single resonant peak that appears in the transmissivity for the barrier thickness of 5.0 nm. The resonant peak occurs at $E_1 = 0.106$ eV and its associated lifetime is $\tau_1 = 0.642$ ps. The resonant energy calculated by the complex energy technique is 0.08 eV. The values computed by the two methods are very close to each other. The resonant lifetimes calculated by the complex energy technique is 0.64 ps and that found by the transfer matrix technique is 0.642 ps which are in good agreement with that calculated by Shao et al. [30]. The value of lifetime obtained by Sollner et al. [31] is 0.60 ps. Sollner et al. addressed that the high-frequency values measured with far IR lasers prove that the charge transport is faster than about 1.0×10^{-13} s. The comparisons with both experimental and theoretical data confirm the validity of our results.

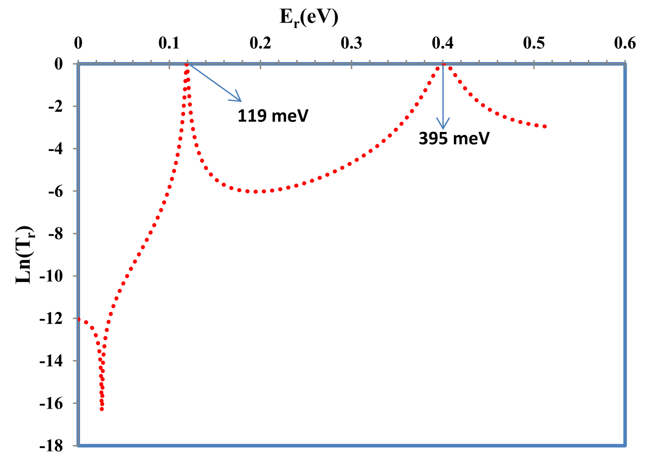

Fig. 9 Natural logarithmic transmission coefficients for nanoscale AlGaAs/GaAs double-barrier heterostructures versus quasi-resonant energy at T = 300 K for a = 5.0 nm, b = 2.0 nm, $m_1 = 0.067$, $m_2 = m_1 + 0.083$ x, where x = 0.5, and $V_0 = 0.5$ eV

The calculated quasi-resonant energy and associated lifetimes obtained for nanoscale AlGaAs/GaAs double-barrier heterostructures for a = 1.5 nm, b = 2.0 nm, $m_1 = 0.069$, $m_2 = m_1 + 0.083 \times$ with Al centration of x = 0.3, and barrier height of $V_0 = 0.24$ eV are listed in Table 6. The variation of the natural logarithm of the transmission coefficients for AlGaAs/GaAs double-barrier heterostructures at T = 300 K with resonant energy for a = 3.0 nm,

Table 4 Calculated quasi-resonant energy and quasi-lifetimes for AlGaAs/GaAs double-barrier heterostructures for a = 5.0 nm, $m_1 = 0.067$, $m_2 = m_1 + 0.083 \times$ with x = 0.5, and $V_0 = 0.5$ eV

b(nm)	Present work								Experiment Ref. [29]			
	Complex energy technique				Transfer matrix technique							
	E_{r1} (meV)	τ_1 (ps)	E_{r2} (meV)	τ_2 (ps)	E_{r1} (meV)	τ_1(ps)	E_{r2} (meV)	τ_2 (ps)	E_{r1} (meV)	τ_1 (ps)	E_{r2} (meV)	τ_2 (ps)
2.0	93.91	0.253	376.89	0.024	119	0.217	395	0.017	92	0.254	412	0.024

Table 5 Calculated quasi-resonant energy and quasi-lifetime for nanoscale AlGaAs/GaAs double-barrier heterostructures for a = 5.0 nm, $m_1 = m_2 = 0.067$, and $V_0 = 0.23$ eV

b(nm)	Complex energy technique		Transfer matrix technique		Experimental data Ref. [30]		Experimental data Ref. [31]	
	E_{r1} (eV)	τ_1 (ps)	E_{r1} (eV)	τ_1 (ps)	E_{r1} (eV)	τ_1 (ps)	E_{r1} (eV)	τ_1 (ps)
5.0	0.08	0.64	0.106	0.642	–	0.64	–	0.60

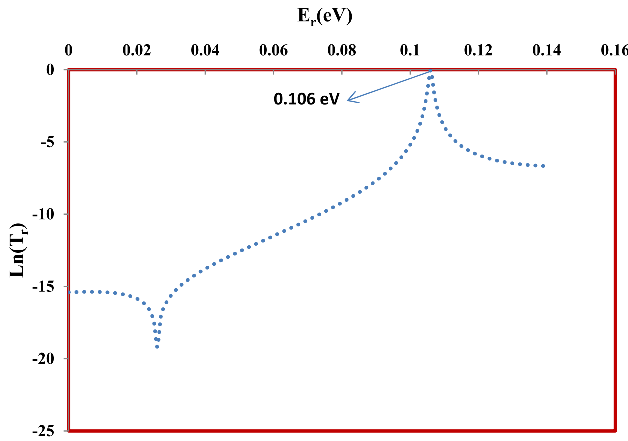

Fig. 10 Natural logarithmic transmission coefficients for AlGaAs/GaAs double-barrier heterostructures at T = 300 K versus quasi-resonant energy for a = 5.0 nm, b = 5.0 nm, $m_1 = m_2 = 0.067$, and $V_0 = 0.23$ eV

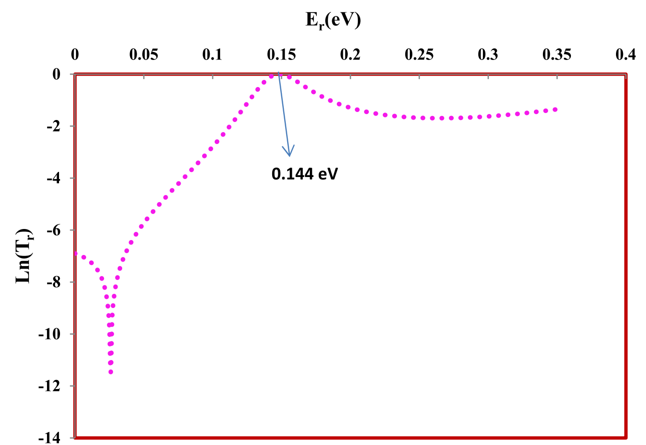

Fig. 11 Natural logarithmic transmission coefficients for nanoscale AlGaAs/GaAs double-barrier heterostructures versus resonant energy at T = 300 K for a = 3.0 nm, b = 2.0 nm, $m_1 = 0.069$, $m_2 = m_1 + 0.083$ x, x = 0.3, and $V_0 = 0.24$ eV

b = 2.0 nm, $m_1 = 0.069$, $m_2 = m_1 + 0.083 \times$ with Al concentration of x = 0.3, and $V_0 = 0.24$ eV is presented in Fig. 10. In Fig. 10 there is a single resonant peak that appears in the transmissivity for the value of the barrier thickness of 2.0 nm. The resonant peak occurred at $E_1 = 0.144$ eV and its associated lifetime is $\tau_1 = 1.63 \times 10^{-14}$ s. The complex energy technique gives quasi-resonant energy of 0.12 eV and the associated lifetime is 1.77×10^{-14} s. This implies that the present two techniques give fairly similar values. Capasso and Richard [32] obtained the quasi-resonant energy of 0.119 eV and the associated quasi-lifetime of 1.0×10^{-14} s. The present results are in excellent agreement with the experimental values obtained by Capasso and Richard [32] (Fig. 11).

4 Conclusion

The calculations for nanoscale resonant tunneling in the group of nanoscale double-barrier resonant tunneling systems composed of ZnSe/BeTe, AlAs/GaAs, InGaAs/AlInAs, and AlGaAs-GaAs heterostructure semiconductors are obtained for the transfer matrix and complex energy methods. The validity and accuracy of these two techniques are proved by significant comparisons with experimental data and various numerical approaches now in use. Our findings are in excellent accord with the available experimental and theoretical values. In the recent decade, more attention is paid to the fabrication of nanoscale heterostructures composed of

Table 6 Calculated quasi-resonant energy and lifetimes obtained for nanoscale AlGaAs/GaAs double-barrier heterostructures for a = 1.5 nm, $m_1 = 0.069$, $m_2 = m_1 + 0.083 \times$ with x = 0.3, and $V_0 = 0.24$ eV

b(nm)	Complex energy technique		Transfer matrix technique		Experiment Ref. [32]	
	E_{r1} (eV)	τ_1 (s)	E_{r1} (eV)	τ_1 (s)	E_{r1} (eV)	τ_1 (s)
2.0	0.12	1.77×10^{-14}	0.144	1.63×10^{-14}	0.119	1.0×10^{-14}

semiconductors of abrupt bandgaps (such as quantum wells, dots, and wires) for novel optoelectronic devices for industrial applications and our daily uses and to enhance the performance of these devices. Nanoscale DBRTHS's are types of these devices and still attract attention in industry and daily use, so the present work is aiming to analyze theoretically some of the composition semiconductors fabricating these devices and to ease the handling of their electronic properties by considering two important widely used techniques based on the effective mass theory, the first is the transfer matrix method that determines the resonant energy from the peak appears in the transmission curve and another formula to determine the corresponding lifetime. The second one is the complex energy technique which is direct and easy to manipulate and detects the quasi-resonant energy and its associated lifetime from the imaginary part of the root that arises from the solution of the transcendental equations given in Eqs. 12 and 17. The present comparative analysis shows good predictions of the quasi-energy and its associated quasi-lifetime for both methods and with those experimental and published data. But the complex energy method is better in both its accuracy and handling, so we recommend it for examining the electronic properties of these nanoscales devices and other novel low-dimensional heterostructures.

Author contributions

All authors read and approved the final manuscript. Elkenany and Elabsy contributed to the formal analysis, methodology, and writing of the original draft.

Funding

Open access funding provided by The Science, Technology & Innovation Funding Authority (STDF) in cooperation with The Egyptian Knowledge Bank (EKB). Not applicable.

Data availability

All data that support the findings of this study are included within the article (and any supplementary files).

Declarations

Conflict of interest The authors declare no conflict of interest.

Research involving human participants and/or animals Not applicable.

Open Access This article is licensed under a Creative Commons Attribution 4.0 International License, which permits use, sharing, adaptation, distribution and reproduction in any medium or format, as long as you give appropriate credit to the original author(s) and the source, provide a link to the Creative Commons licence, and indicate if changes were made. The images or other third party material in this article are included in the article's Creative Commons licence, unless indicated otherwise in a credit line to the material. If material is not included in the article's Creative Commons licence and your intended use is not permitted by statutory regulation or exceeds the permitted use, you will need to obtain permission directly from the copyright holder. To view a copy of this licence, visit http://creativecommons.org/licenses/by/4.0/.

References

1. R. Kudrawiec, D. Hommel, Appl. Phys. Rev. **7**, 41314 (2020)
2. J. Fast, U. Aeberhard, S.P. Bremner, H. Linke, Appl. Phys. Rev. **8**, 21309 (2021)
3. Y. Xu, Q. Lin, Appl. Phys. Rev. **7**, 11315 (2020)
4. D. Dastan, J. At. Mol. Condens. Matter Nano Phys. **2**, 109 (2015)
5. W. Hu, T. Li, X. Liu, D. Dastan, K. Ji, P. Zhao, J. Alloys Compd. **818**, 152933 (2020)
6. R. Shakoury, A. Arman, Ş Ţălu, D. Dastan, C. Luna, S. Rezaee, Opt. Quantum Electron. **52**, 1 (2020)
7. L. Esaki, R. Tsu, IBM J. Res. Dev. **14**, 61 (1970)
8. G. Bastard, E.E. Mendez, L.L. Chang, L. Esaki, Phys. Rev. B **28**, 3241 (1983)

9. S. Vatannia, G. Gildenblat, IEEE J. Quantum Electron. **32**, 1093 (1996)
10. Y. Tsuji, M. Koshiba, Microelectronics J. **30**, 1001 (1999)
11. K. Hayata, M. Koshiba, K. Nakamura, A. Shimizu, Electron. Lett. **24**, 614 (1988)
12. B. Jonsson, S.T. Eng, IEEE J. Quantum Electron. **26**, 2025 (1990)
13. K. Mukherjee, N. R. Das, In *2009 4th Int. Conf. Comput. Devices Commun* (IEEE, 2009), pp. 1–4.
14. A.K. Ghatak, K. Thyagarajan, M.R. Shenoy, IEEE J. Quantum Electron. **24**, 1524 (1988)
15. K. Talele, D. Patil, Prog. Electromagn. Res. **81**, 237 (2008)
16. A.R. Sugg, J.-P. Leburton, IEEE J. Quantum Electron. **27**, 224 (1991)
17. H. Xu, F. Zhang, G. Chen, Phys. Status Solidi **183**, K37 (1994)
18. H. Yamamoto, Y. Kanie, K. Taniguchi, Phys. Status Solidi **167**, 571 (1991)
19. A. Zarifkar, A.M. Bagherabadi, IJCSNS **8**, 266 (2008)
20. M.O. Vassell, J. Lee, H.F. Lockwood, J. Appl. Phys. **54**, 5206 (1983)
21. D.X. Xu, G.D. Shen, M. Willander, G.V. Hansson, J. Appl. Phys. **71**, 3859 (1992)
22. A.M. Elabsy, E.B. Elkenany, Phys. B Condens. Matter **632**, 413711 (2022)
23. K. Araki, J. Appl. Phys. **62**, 1059 (1987)
24. H.G. Abdelwahed, *MSc Diss* (Mansoura Univ, Egypt, 2003)
25. T.B. Bahder, C.A. Morrison, J.D. Bruno, Appl. Phys. Lett. **51**, 1089 (1987)
26. S.S. Allen, S.L. Richardson, Phys. Rev. B **50**, 11693 (1994)
27. M. Shen, W. Cao, Mater. Sci. Eng. B **103**, 122 (2003)
28. U. Lunz, M. Keim, G. Reuscher, F. Fischer, K. Schüll, A. Waag, G. Landwehr, J. Appl. Phys. **80**, 6329 (1996)
29. H.Z. Xu, Y. Okada, Phys. B Condens. Matter **305**, 113 (2001)
30. Z. Shao, W. Porod, C.S. Lent, D.J. Kirkner, J. Appl. Phys. **78**, 2177 (1995)
31. T. Sollner, W.D. Goodhue, P.E. Tannenwald, C.D. Parker, D.D. Peck, Appl. Phys. Lett. **43**, 588 (1983)
32. F. Capasso, R.A. Kiehl, J. Appl. Phys. **58**, 1366 (1985)

Publisher's Note Springer Nature remains neutral with regard to jurisdictional claims in published maps and institutional affiliations.